Chapter 4

Contrast-enhanced MRI-derived Scar Patterns and Associated Ventricular Tachycardias in Nonischemic Cardiomyopathy:

Implications for the Ablation Strategy

Sebastiaan R.D. Piers, MD, Qian Tao, PhD, Carine F.B. van Huls van Taxis, MD, Martin J. Schalij, MD, PhD, Rob J. van der Geest, PhD, Katja Zeppenfeld, MD, PhD

Circulation: Arrhythmia & Electrophysiology 2013;6(5):875-83

ABSTRACT

Background

There are limited data on typical arrhythmogenic substrates and associated ventricular tachycardias (VT) in patients with nonischemic cardiomyopathy (NICM). The substrate location may have implications for the ablation strategy.

Methods and results

Nineteen consecutive patients with NICM (age 58±14years, 79% male, LVEF 41±11%) who underwent contrast-enhanced MRI (CE-MRI) and VT ablation were included. Based on 3D CE-MRI-derived scar reconstructions, 8 patients (42%) had predominant basal anteroseptal scar, 9 (47%) predominant inferolateral scar and 2 (11%) other scar types. Three distinct VT morphologies (≥1 of 3 inducible in 16/19 patients) were associated with underlying scar type. In 9 patients with anteroseptal scar-related VT (8/9 predominant scar, 1/9 non-predominant), ablation target sites (defined as sites with ≥11/12 pacemap, concealed entrainment or VT termination during ablation) were located in the aortic root and/or anteroseptal left ventricular endocardium in 8 (89%) and in the anterior cardiac vein in 1 (11%), with additional target sites at the right ventricular septum in 2 (22%) and at the epicardium in 1 (11%). In contrast, in 8 patients with predominant inferolateral scar-related VT, target sites were located at the epicardium in 5 (63%) and in the endocardial, inferolateral LV in 3 (37%).

Conclusion

Two typical scar patterns (anteroseptal and inferolateral) account for 89% of arrhythmogenic substrates in patients with NICM. Three distinct VT morphologies are highly suggestive for the presence of these scars. Anteroseptal scars were in general most effectively approached from the aortic root or anteroseptal LV endocardium, whereas inferolateral scars frequently required an epicardial approach.

INTRODUCTION

The substrate for ventricular tachycardia (VT) in patients with non-ischemic cardiomyopathy (NICM) is typically located near the base of the left ventricle (LV) close to the valve annuli, with an intramural or subepicardial distribution pattern.[1-3] Isolated septal scars have been reported in approximately 12% of patients,[2] but may be difficult to detect by electroanatomical mapping (EAM),[2,4] thereby underestimating its prevalence. Viable myocardium overlying the substrate may prevent scar detection by bipolar EAM.[2,5] Unipolar voltage mapping has been suggested to have a larger 'field of view' than bipolar voltage mapping, allowing detection of subepicardial scars during endocardial mapping.[6] The exact size of this 'field of view' is however unclear and has not been validated by contrast-enhanced magnetic resonance imaging (CE-MRI), which is considered to be the gold standard to detect scar.

CE-MRI derived 3-dimensional (3D) scar reconstructions may provide insights into the geometry of the arrhythmogenic substrate[4] and its spatial relation to anatomical structures, which may have implications for the procedural strategy, the required access and potential limitations for ablation.

The 12-lead morphology of scar-related VT depends on 3D scar geometry and VT exit site, and may help to identify the substrate in patients in whom CE-MRI is not available. Distinct VT morphologies have been described in selected patients with NICM and isolated septal scars,[2] but not in other scar types.

The aims of the present study were 1) to identify typical MRI-derived scar patterns and the associated 12-lead VT morphologies in consecutive patients with NICM who underwent CE-MRI and VT ablation, 2) to evaluate its implications for the ablation strategy and 3) to analyze the value of bipolar and unipolar endocardial voltage mapping to detect the CE-MRI-derived VT substrate in patients with NICM.

METHODS

Patients

The study sample consisted of 19/21 consecutive patients with NICM who underwent CE-MRI and VT ablation. Two patients with poor CE-MRI image quality were excluded. Patients with coronary artery disease (>50% stenosis, assessed by coronary angiography in all patients), congenital heart disease, hypertrophic, arrhythmogenic right ventricular and restrictive cardiomyopathy, LV noncompaction, (sub)acute myocarditis, cardiac sarcoidosis, tachycardia-induced cardiomyopathy or primary valvular abnormalities were excluded. All patients were treated according to the routine clinical protocol and provided informed consent.

CE-MRI acquisition and processing

Contrast-enhanced MRI was performed on a 1.5 T Gyroscan ACS-NT/Intera MR system (Philips Medical Systems, Best, the Netherlands). A standardized protocol was followed, including cine MRI in long- axis (two- and four-chamber views) and short-axis covering the LV. In addition, the proximal aorta was imaged using a black-blood turbo spin-echo sequence. Contrast-enhanced images were acquired 15 min after bolus injection of gadolinium (Magnevist; Schering, Berlin, Germany; 0.15 mmol/kg) using a 3D turbo-field echo sequence with parallel imaging. The heart was imaged in one or two breath-holds with 20–24 imaging levels (dependent on heart size) in short-axis views. Images were acquired 600–700ms after the R-wave.

Using Mass research software, the centerline of the proximal coronary arteries was manually defined in the black-blood spin-echo image stack. The aortic, endocardial and epicardial contours were semi-automatically detected on short axis views and converted into 3D meshes. Myocardial tissue with 35-50% and ≥50% of maximal signal intensity were considered grey zone and core scar, respectively. The LV endocardial and epicardial meshes were color-coded for scar transmurality in the inner and outer half of the wall, respectively. All meshes were imported into the CARTO system using IPE-software (Figure 1).

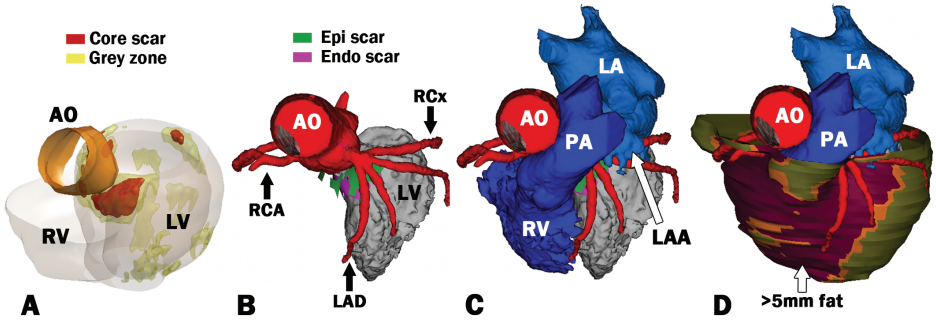

Figure 1. Example of a MRI-derived basal anteroseptal scar
In panel A the core scar is displayed in red, the grey zone in yellow. Based on fused CT- and MRI-derived information, the scar cannot be reached from the epicardium due to overlying coronary arteries (panel B), the pulmonary artery (panel C) and epicardial fat (panel D). In panels B and C, the scar in the endocardial half of the wall is displayed in purple, scar in the epicardial half in green.

CT acquisition and processing

Prior to epicardial ablation electrocardiogram-gated cardiac CT imaging was performed with an intravenous iodinated contrast agent. The endocardial, epicardial and pericardial contours were manually traced on short-axis reformatted CT slices to create 3D meshes color-coded for fat thickness (distance between epicardial and pericardial contours).[7,8] Subsequently, the original CT data and the 3D meshes were imported into the mapping system. These images were used during epicardial VT ablation procedures to avoid RF

applications in the close vicinity of coronary arteries and to provide detailed information on epicardial fat thickness, which may facilitate the interpretation of electrograms and explain ineffective RF applications.[7]

Electrophysiological evaluation

Anti-arrhythmic drugs were discontinued for at least 5 half-lives with the exception of amiodarone (n=2). Programmed electrical stimulation was performed before sedation and opioid administration. The simulation protocol consisted of 3 drive cycle lengths (600, 500 and 400ms) with 1-3 ventricular extrastimuli (≥200ms) from 2 right ventricular (RV) sites and burst pacing (CL≥200ms), repeated with isoproterenol (2-10μg/min) when necessary. Positive endpoint was induction of a sustained monomorphic VT (>30s or requiring termination because of hemodynamic compromise).

VT morphologies

All induced sustained monomorphic VTs were categorized as right or left bundle branch block-like (RBBB or LBBB) morphology (defined as predominant R or S V1), inferior or superior axis (predominant R or S in aVF), left or right axis (predominant R or S in I) and precordial transition (first lead with a predominant R or S for LBBB and RBBB VTs, respectively).

Electroanatomical mapping, real-time image integration and ablation

Epicardial access was obtained through a subxyphoid puncture. Electroanatomical bipolar and unipolar voltage mapping was performed using a 3.5mm irrigated-tip catheter (2mm ring electrode, 1mm interelectrode spacing; NaviStar ThermoCool, Biosense Webster Inc, Diamond Bar, CA, USA) and the CARTO system. Electrograms were filtered at 30-400Hz (bipolar) and 1-240Hz (unipolar). Limited EAM of the aortic root was performed and the position of the left main coronary artery, confirmed by undiluted contrast injection through the mapping catheter, was tagged on the map. The LV was mapped retrogradely focusing on the MRI-derived scar areas. The RV was mapped if indicated. CE-MRI-derived images were aligned with the EAM using the left main landmark. Then, the LV surfaces were aligned with the translation tool until the lowest mean surface registration error was reached. The CT-derived coronary anatomy and epicardial fat meshes were integrated with the EAM in patients who underwent epicardial mapping, as previously described.[8]

Potential re-entry circuit sites targeted for ablation were identified based on activation mapping and entrainment mapping for stable VT. For unstable VT, the area of interest was identified by substrate mapping and pace mapping. Then, VT was reinduced and briefly mapped in an attempt to identify diastolic activity and terminate the VT by ablation. For analyses purposes, ablation target sites were defined as sites with 1) ≥11/12

Table 1. Baseline characteristics and procedural data

	All patients (n=19)	Predominant anteroseptal scar (n=8)	Predominant inferolateral scar (n=9)
Age	58±14	61±12	56±16
Male	15(79%)	7(88%)	7(78%)
LV ejection fraction, %	41±11	40±8	44±15
LV end-diastolic volume, mL	230±73	224±36	237±102
History of atrial flutter/fibrillation	3(16%)	2(25%)	1(11%)
BMI, kg/m^2	26.4±4.2	27.8±5.2	26.2±2.8
Diabetes mellitus	2(11%)	0(0%)	2(22%)
eGFR < 60 mL/min	2(11%)	1(13%)	1(11%)
Number of VTs induced	2(1-3)	3(2-6)	2(1-4)
BBR VT	0(0%)	0(0%)	0(0%)
Unstable VT	14(74%)	5(62%)	7(78%)
Mean CL of induced VTs	298±69	308±75	304±68
LV endocardial mapping	19(100%)	8(100%)	9(100%)
Low bipolar voltage area, cm^2	8.7(3.1-15.0)	9.9(4.1-14.1)	5.1(0.35-15.7)
Low unipolar voltage area, cm^2	14.4(7.1-27.9)	12.9(7.3-27.7)	14.4(0.7-27.5)
Electrogram abnormalities*	11/6/2	5/3/0	5/3/1
Epicardial mapping	11(58%)	3(38%)	7(78%)
Low bipolar voltage area, cm^2	28.4(20.0-41.3)	20.0(16.6-22.7)	34.1(28.4-46.8)
Low unipolar voltage area, cm^2	47.1(16.4-55.9)	16.4(15.0-16.6)	51.6(35.0-55.9)
Electrogram abnormalities*	9/1/1	2/0/1	7/0/0
Epicardial ablation	8(42%)	2(25%)	6(67%)
Procedural duration, minutes	218±83	230±117	225±44
Fluoroscopy time, minutes	49±19	55±26	46±7
Acute outcome			
Complete success	10(53%)	4(50%)	5(56%)
Partial success	6(32%)	3(38%)	3(33%)
Failure	3(16%)	1(13%)	1(11%)

Other scar types in 2 patients are not described separately

*Specific (double, fragmented or late potential)/only other abnormal/none

pace map and/or 2) concealed entrainment suggestive for a central isthmus or exit site and/or 3) VT slowing and termination during ablation.

At the epicardium, ablation was usually withheld when the estimated distance to a coronary artery was <5mm, as assessed by integrated CT-derived coronary anatomy and coronary angiography.[7] High output pacing (10mA, 2ms) was performed to determine the location of the phrenic nerve. Radiofrequency (RF) energy was applied at 30-45W

(maximum temperature 45°C, flow 20-30ml/min, 60s) for endocardial sites and up to 50W (flow 20ml/min) for epicardial sites.

Acute and long-term outcome

After ablation, the entire stimulation protocol was repeated. Isoprenaline was administered if required to induce VT before ablation. Complete procedural success was defined as non-inducibility of any sustained monomorphic VT; partial success as elimination of the clinical VT but inducibility of ≥1 nonclinical VT; failure as inducibility of the clinical VT. Patients were followed at 3, 6 and 12 months and at 6- to 12-monthly intervals thereafter.

Contrast-enhanced MRI-derived 3D scar reconstructions

Based on the short-axis slices, 3D scar reconstructions were created (MATLAB software, version 2009b). For each patient, the MRI-derived scar transmurality (including core and grey zone) was calculated and displayed on a bull's eye image containing the 17 LV segments. Based on the reconstructions, the locations of the predominant (i.e. largest) scar and of additional scars (defined as scars involving ≥25% of a remote segment) were assessed. The scar distribution within the LV wall was determined by calculating the average endocardial and epicardial viable layers for each scar.

After the procedure, all mapping points were superimposed on the MRI-derived 3D scar reconstruction. For each point, a 5mm-diameter transmural cylinder was created and the presence of late enhancement and the thickness of the endocardial viable layer were assessed.

Statistical analysis

Categorical variables are displayed as number (percentage) and continuous variables as mean±SD or median (first-to-third quartile [Q1-to-Q3]). Categorical variables were compared using the Chi-square test or Fisher's exact test. Continuous variables were compared using the Student's t-test when normally distributed, or the Mann-Whitney U test when non-normally distributed. Mapping point-based receiver operating characteristic curve analysis was performed to determine the optimal cut-off values of bipolar and unipolar voltage for scar detection, defined as the values maximizing the sum of sensitivity and specificity. An additional cutoff value with a fixed specificity of 80% was calculated for unipolar voltage. The bipolar and unipolar voltage of mapping points at scars with an endocardial viable layer of 0-2mm, 2-4mm, 4-6mm, 6-8mm, >8mm and non-scar areas were averaged in each patient. Paired T-tests were subsequently performed to analyze the difference between the average voltage at non-scar areas and the average voltage at scar areas with different endocardial viable layers in the same patient. All analyses were performed with SPSS v20.0 (SPSS Inc., Chicago, Illinois). All p-values are two-sided and p-values <0.05 were considered significant.

RESULTS

Patients

Nineteen patients (age 58±14 years, 15 [79%] male, LV ejection fraction 41±11%) underwent VT-ablation with CE-MRI integration. In 11 patients who underwent epicardial mapping, CT-derived coronary anatomy and epicardial fat thickness were also integrated. Baseline characteristics are summarized in Table 1. None of the patients had documented pericarditis or myocarditis. Three patients (16%) had a family history of NICM/sudden cardiac death.

Typical MRI-derived scar patterns

As illustrated by the bull's eye plot color-coded for the average MRI-derived scar transmurality (Figure 2), two typical scar patterns could be identified. One was located in the basal anteroseptal segment (referred to as *anteroseptal scar*) and the other in the basal/mid inferior, inferolateral and/or lateral segments (referred to as *inferolateral scar*). A predominant anteroseptal scar was present in 8/19 patients (42%) and a predominant inferolateral scar in 9 (47%, Figure 3). Of the remaining 2 patients (11%), one had a subepicardial inferoapical scar and the other had a subepicardial scar along the anterior interventricular groove.

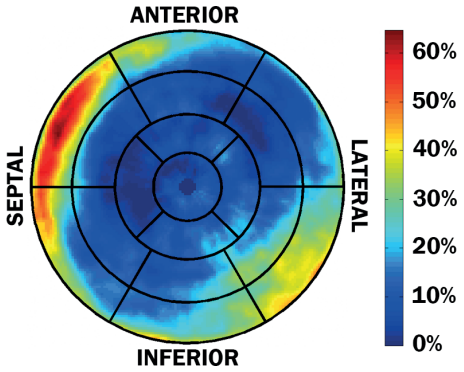

Figure 2. Scar distribution
In each patient the 3D scar reconstruction was used to create a 17-segment bull's eye image displaying the scar transmurality. These data were subsequently averaged to create a single bull's eye image color-coded for the average scar transmurality in all patients, which is displayed continuously from highest (in red) to lowest (in blue).

Two of 8 patients (25%) with a predominant anteroseptal scar also had a smaller inferolateral scar, and 6/9 patients (67%) with a predominant inferolateral scars also had a smaller anteroseptal scar.

Distinct ECG patterns of VTs

A total of 60 VTs were induced (median 2 VTs per patient; Q1-to-Q3, 1–3). Three distinct ECG patterns were observed (Figure 4):

1) RBBB, left/right inferior axis, positive concordance (Panel A) in 12 induced VTs (20%) in 8 patients (42%);
2) LBBB, left/right inferior axis, early (≤V3) precordial transition (Panel B) in 7 induced VTs (12%) in 6 patients (32%);

3) RBBB, right inferior/superior axis, late (≥V5) precordial transition (Panel C) in 6 induced VTs (10%) in 6 patients (32%);

Together, 25 of 60 VTs (42%) had one of these three morphologies. All patients with type 1 or type 2 VTs had anteroseptal scar; all patients with type 3 VTs had inferolateral scar. A less distinct ECG pattern, LBBB VTs with a superior axis and varying transition, was observed in patients with anteroseptal, inferolateral or non-typical scar extending to the inferoseptum. Sixteen of 19 patients (84%) had at least one type 1, 2 or 3 VT. The remaining 3 patients (16%) had extension of the scar on CE-MRI consistent with the VT morphology.

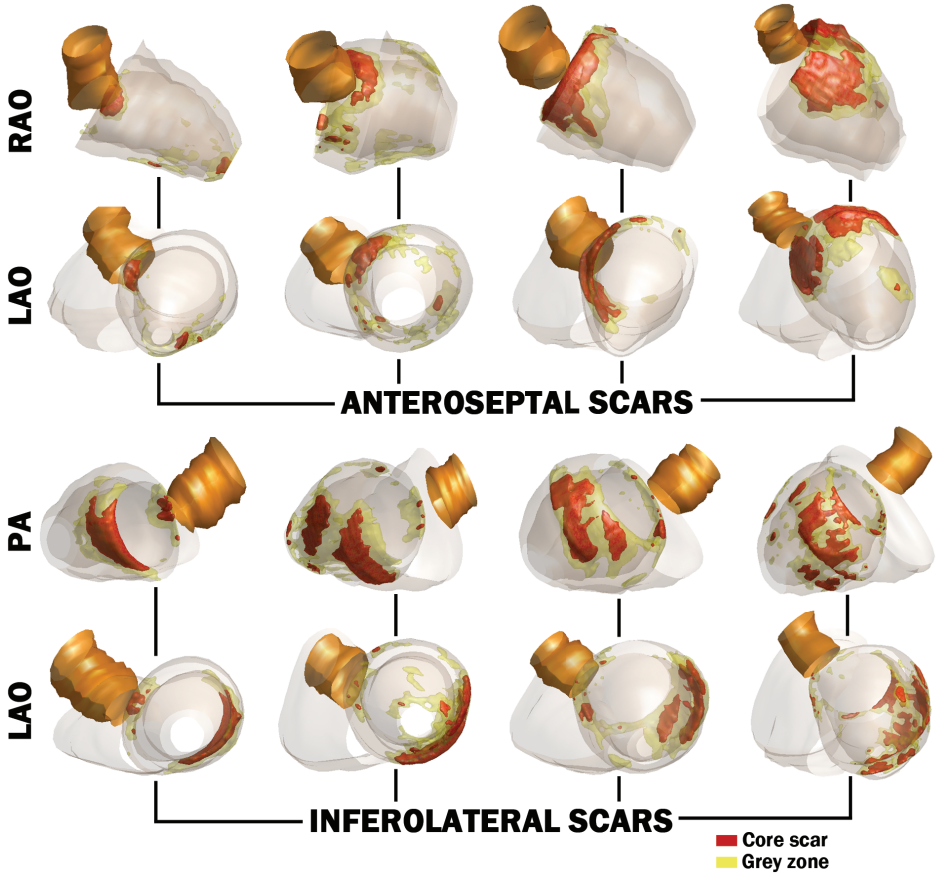

Figure 3. Typical scars

Typical examples of basal anteroseptal scars are shown in right anterior oblique (RAO) and left anterior oblique (LAO) views, typical inferolateral scars in posterior-anterior (PA) and left anterior oblique (LAO) views. Red indicates core scar; yellow, grey zone.

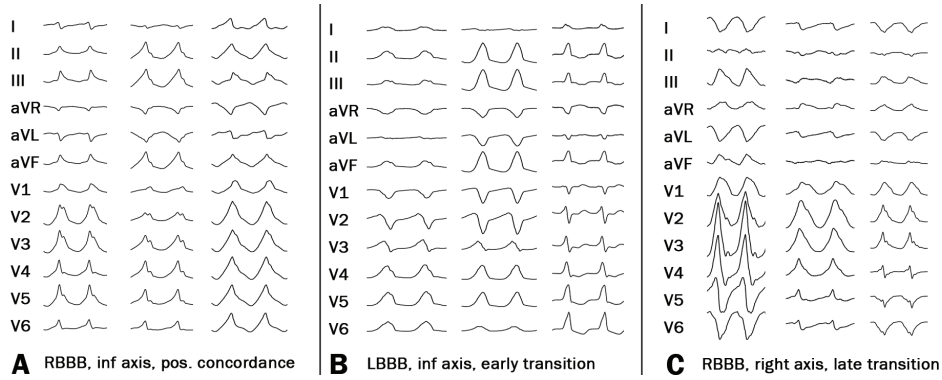

Figure 4. Distinct ECG patterns of ventricular tachycardias
RBBB denotes right bundle branch block; inf, inferior; LBBB, left bundle branch block.

Electroanatomical substrate mapping and ablation target sites

Procedural data are summarized in Table 1. CE-MRI-derived data were successfully integrated in all patients (mean registration error 3.7±0.8mm). Substrate mapping of the LV (all patients, mean 128 points) and the epicardium (11 patients [58%], mean 155 points) was performed focusing on the area of interest as identified by MRI (Table 1 and Figure 5).

A ≥11/12 pacemap was obtained for 31 VTs (52%). Diastolic potentials were identified during 26 VTs (43%) and for 7 VTs (12%) concealed entrainment was suggestive for a central isthmus or exit site (stimulus-QRS 43 – 254ms). Eighteen VTs (30%) slowed and terminated during RF applications after a median of 9 seconds (Q1-to-Q3, 7–13 sec) without premature ventricular contraction. Overall, ablation target sites were identified for 40 VTs (67%). The locations of these target sites are displayed in Figure 6. All target sites were located within 10mm of the CE-MRI-derived scar area.

In 9 patients with basal anteroseptal scar-related VT (predominant in 8), target sites were located in the aortic root and/or basal anteroseptal LV endocardium in 8 (89%) and in the anterior cardiac vein in 1 (11%), with additional target sites at the RV septum in 2 (22%) and at the basal anterior epicardium in 1 (11%).

In contrast, in 8 patients inferolateral scar-related VT (all predominant scars), target sites were located at the inferolateral epicardium in 5 patients (63%) and in the inferolateral endocardial LV in 3 (37%, both endocardial and epicardial target sites in one), with an additional target site at the epicardial RV outflow tract in one. No target sites could be identified in one patient.

Anatomical limitations of mapping and ablation

In patients with a predominant anteroseptal scar, ablation was limited by the proximity of the proximal conduction system in 2 (25%) and by the left main ostium in another 2 (25%). Based on integrated CT- and MRI-derived information, the entire scar could not

be reached from the epicardium due to the RV, pulmonary artery, overlying coronary arteries and/or epicardial fat in 5 patients (63%, Figure 1) and only part of the scar could be

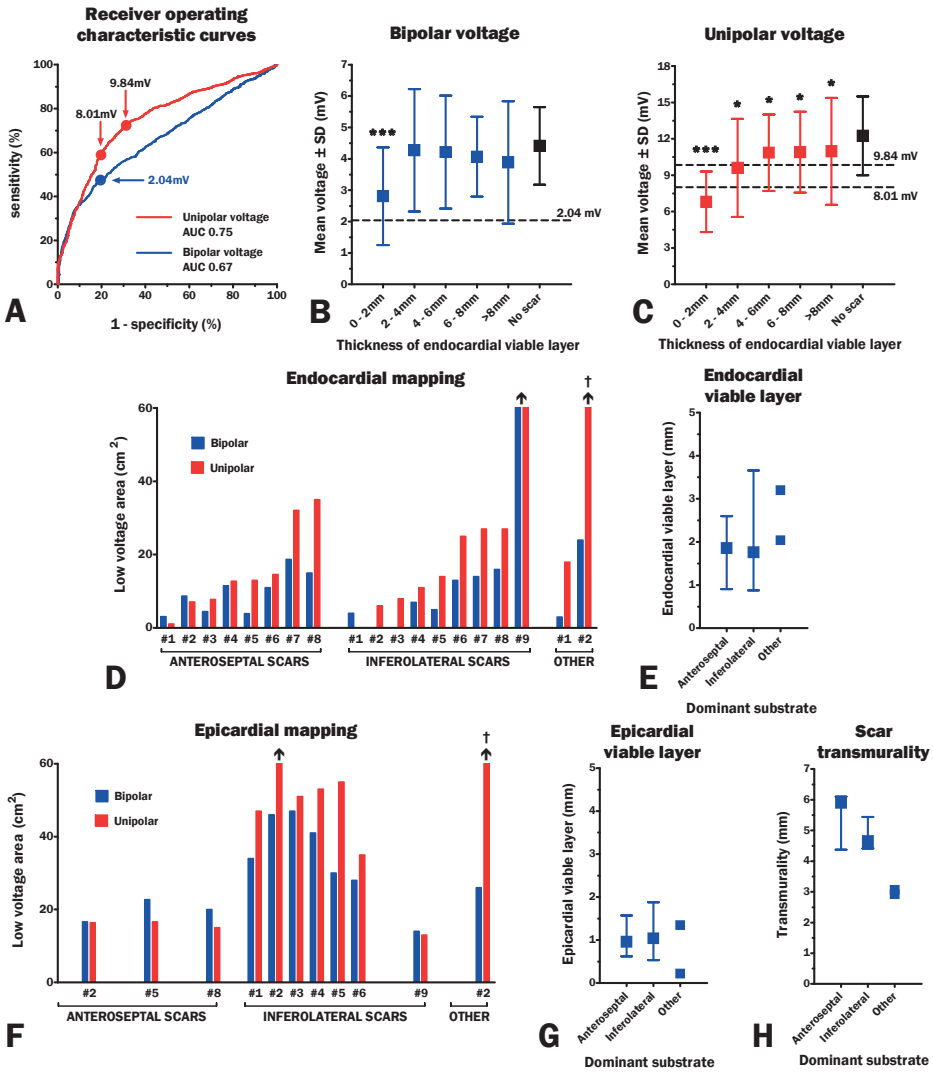

Figure 5. Bipolar vs. unipolar voltage mapping and scar features

Panel A: Receiver operating characteristic curve analysis for bipolar/unipolar voltage and MRI-derived scar. Panel B: Endocardial bipolar voltage is decreased only when the endocardial viable layer is <2mm thick. Panel C: Endocardial unipolar voltage was affected by scar involving the endocardial 4mm and, but less pronounced, by scar >4mm from the endocardium. Panel D: Endocardial low voltage areas. Panel E, G and H: Subendocardial and subepicardial viable layers and scar transmurality. Panel F: Epicardial low voltage areas in patients who underwent epicardial mapping. *** indicates $p < 0.001$ vs. no scar; *, $p < 0.05$ vs. no scar; †, One patient with a relatively thin LV wall (6.3±1.5mm) had low unipolar voltage at the entire endocardium and epicardium. AUC denotes area under the curve.

reached in the remaining 3 patients (37%). In 3 patients with an anteroseptal substrate epicardial mapping and ablation was performed after image integration. The expected epicardial accessibility of the scar was confirmed in these patients (only part of the scar reachable in 2, the entire scar not reachable in one).

In patients with a predominant inferolateral scar and endocardial ablation target sites, endocardial ablation was not limited. Based on integrated CT-derived information, coronary angiography and high-output pacing, RF applications had to be withheld at the epicardium due to the right coronary artery or the obtuse marginal branch in 3/7 patients (43%) and due to phrenic nerve capture in one.

Contrast-enhanced MRI-derived 3D scar reconstructions

A total of 2444 points acquired in the LV were projected on 3D scar reconstructions. Scar was present at 1146 sites (47%). For endocardial bipolar voltage the optimal cut-

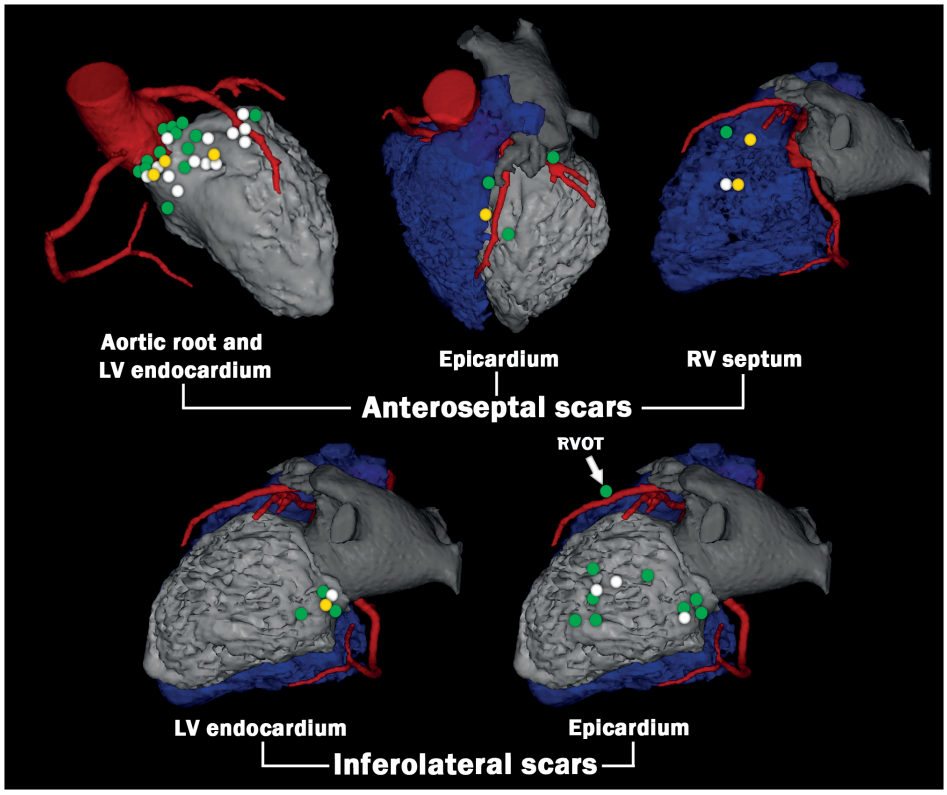

Figure 6. Ablation target sites.
Ablation target sites in all patients projected on the computed tomography-derived anatomy of a single patient. Green points indicate ≥11/12 pace maps; yellow points, concealed entrainment sites suggestive for a diastolic part of the re-entry circuit; white points, VT termination sites. LV denotes left ventricle; RV, right ventricle; RVOT, right ventricular outflow tract.

off value to differentiate between scar and viable myocardium was 2.04mV (AUC 0.67, sensitivity 48%, specificity 81%, Figure 5). For endocardial unipolar voltage the optimal cut-off value was 9.84mV (AUC 0.75, sensitivity 73%, specificity 69%). The specificity could be increased to 80% using a cut-off value of 8.01mV, which resulted in a sensitivity of 59%. Endocardial bipolar voltage was only affected by scar involving the endocardial 2mm, whereas endocardial unipolar voltage was affected by scar involving the endocardial 4mm and, less pronounced, by scar >4mm from the endocardium (Figure 5). Two patients (one with a basal anteroseptal scar and one with an inferolateral scar) had an epicardial scar identified by MRI that significantly exceeded small endocardial bipolar and unipolar low voltage areas (example in Figure 7).

Low bipolar and unipolar voltage areas, thickness of endocardial and epicardial viable layers and average scar transmurality were similar for anteroseptal and inferolateral scars (all p>0.05; Figure 5, panels D-H).

Acute and long-term procedural outcome

Complete success was achieved in 10 patients (53%), partial success in 6 (32%) and ablation failed in 3 (16%). The acute procedural outcome did not differ between patients with a predominant anteroseptal or inferolateral scar (Table 1). Seventeen of 19 patients (90%) were discharged with an implantable cardioverter defibrillator (ICD). During a median 15 (Q1-to-Q3, 11–27) months follow-up, 7/19 patients (37%) had VT recurrence (4/8 with a predominant anteroseptal scar, 2/9 with a predominant inferolateral scar, 1/2 with other scar type). The 6-month VT burden was reduced by ≥75% in 16/19 patients (84%). One patient died due to a lung cancer.

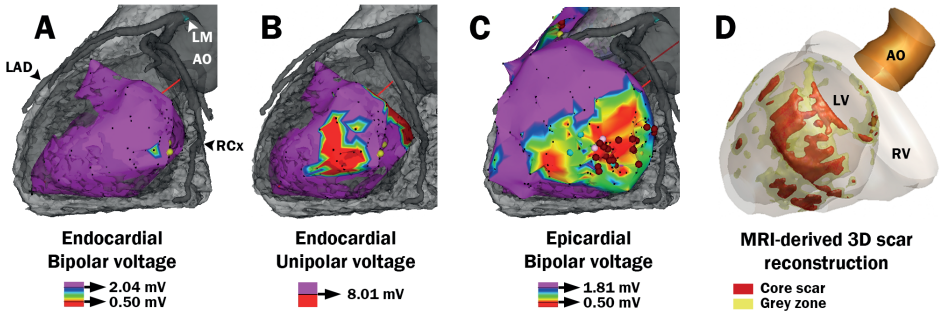

Figure 7. Example of electroanatomical maps and a 3D scar reconstruction

Endocardial bipolar (panel A) and unipolar (panel B) voltage maps, epicardial bipolar voltage map (panel C) with integrated CT-derived anatomy, and the MRI-derived 3D scar reconstruction (panel D). Voltages are color coded as indicated by the color bars. AO indicates aorta; LAD, left anterior descending coronary artery; LM, left main coronary artery; LV, left ventricle; RCx, circumflex coronary artery; RV, right ventricle.

DISCUSSION

In the present study, CE-MRI-derived scar was associated with VT in patients with NICM. Two typical scar patterns (i.e., anteroseptal and/or inferolateral scars) were present in 89% of patients referred for VT ablation. Three distinct 12-lead ECG morphologies of VTs were common and diagnostic for a typical scar pattern. Ablation target sites in patients with a basal anteroseptal scar were mainly identified in the aortic root and the basal anteroseptal LV endocardium, whereas target sites in patients with an inferolateral scar were located at the epicardium in 63% of patients. The typical scar patterns may therefore have implications for the mapping and ablation strategy. Endocardial EAM is insufficient to delineate these scars, as endocardial bipolar voltage was only affected by scar involving the endocardial 2mm, and endocardial unipolar voltage by scar involving the endocardial 4mm and, less pronounced, by scar >4mm from the endocardium.

Typical arrhythmogenic substrates

Prior studies have described arrhythmogenic substrates in NICM, but have not systematically used CE-MRI as a gold standard for scar detection.[2,9] In the current study, the EAM and CE-MRI-derived 3D scar reconstructions allowed a detailed evaluation of the arrhythmogenic substrate.

Importantly, all ablation target sites were located within 10mm of the CE-MRI-derived scar area. A predominant basal anteroseptal scar was present in 42% of patients but often associated with only a small endocardial low bipolar voltage area, difficult to distinguish from a normal low voltage area at the membranous part of the interventricular septum. In this group endocardial target sites could be identified in all but one patient. The ablation was withheld due to the location of the conduction system in one patient and caused expected atrioventricular block in another. Epicardial mapping in the presence of this scar pattern was considered impossible due to or hampered by overlying coronary arteries, fat and the left atrial appendage.

Although basal anteroseptal scars have been described in prior studies and two case reports[2-4,9,10], they are reported to occur in only 11.3% of NICM patients.[2] Based on the current data and two prior studies, these scars may however be difficult to detect by substrate mapping[2,4] and as a result, scar-related VTs may even be mistaken for benign idiopathic outflow tract VTs, which may have important prognostic and therapeutic consequences.[4]

A predominant inferolateral scar was present in 47% of patients but also difficult to detect by endocardial bipolar voltage mapping. Endocardial unipolar voltage mapping allowed improved but still limited scar detection. Epicardial mapping was not limited and epicardial target sites were identified in 63% of these patients. Epicardial ablation was however partly withheld due to coronary arteries and the phrenic nerve.

In the current study, CE-MRI served as a gold standard for LV scar. For both scar patterns endocardial bipolar voltage was only affected by scar involving the endocardial 2mm, whereas endocardial unipolar voltage was affected by scar involving the endocardial 4mm and, less pronounced, by scar >4mm from the endocardium. . Accordingly, the sensitivity for bipolar and unipolar voltage mapping to detect scar in the NICM population is poor with an overall sensitivity of 48% and 59%, respectively. Therefore CE-MRI should be considered in all patients with suspected NICM before VT ablation and ICD implantation.

In only one patient in our study a causative mutation (phospholamban) for NICM has been identified (yet) and none had a history of myocarditis. However, typical septal and/or inferolateral scars have been described in various diseases, such as myocarditis,[11] arrhythmogenic right ventricular cardiomyopathy/dysplasia with LV involvement,[12] laminopathy[13] and Anderson-Fabry disease[14]. Rather than disease specific, these areas may be more vulnerable to various insults resulting in fibrosis and ultimately VT.

Typical 12-lead ECG VT morphologies

At least one of three distinct VT morphologies was observed in 84% of patients and these morphologies were related to the two scar patterns. Documentation of these distinct morphologies may be helpful if CE-MRI is not available. Two typical VT morphologies have been previously described in patients with NICM but only with isolated septal scars, including inferior limb discordance (dominant R in II and dominant S in III, or the opposite) in 16% of VTs, and precordial transition break in V2 (qR/Rs morphology in V1 and V3 but reversal of this in V2) in 24% of VTs.[2] In the current study, each criterion was observed in 5/37 induced VTs (14%) in 2/8 patients (25%) with a predominant anteroseptal scar.

Implications for the procedural strategy

VTs related to basal anteroseptal scar were effectively approached from the aortic root or basal anteroseptal LV endocardium, whereas VTs related to an inferolateral scar often required an epicardial approach. This finding may influence the procedural strategy in patients with NICM and a typical substrate based on imaging or a distinct VT morphology. An initial endocardial approach may be appropriate in patients with a presumed basal anteroseptal substrate. A retrograde approach to the LV may be preferred over an antegrade approach, allowing mapping in the aortic sinus cusps. In patients with an inferolateral scars, epicardial mapping and ablation are likely to be necessary and an initial combined endocardial and epicardial approach may be reasonable.

Limitations

Although the present study demonstrates a clear predilection for scars in the basal anteroseptal and inferolateral segments, there may be nonischemic scar distributions (and associated VT morphologies) that are not identified in this study. The number of patients was limited, as only patients without an implantable device underwent CE-MRI. No ablation target sites could be identified for 33% of VTs, which may be due to intramural circuits or subepicardial circuits in areas covered with fat. Epicardial mapping was not performed in 4 patients with non-complete procedural success because the septal substrate was likely not accessible from the epicardium based on CE-MRI.

CONCLUSION

Basal anteroseptal and inferolateral scars account for 89% of arrhythmogenic substrates in patients with NICM. Typical VT morphologies, observed in 84%, may help to identify the underlying substrate. Basal anteroseptal scars were in general most effectively approached from the aortic root or basal anteroseptal LV endocardium, whereas inferolateral scars frequently required an epicardial approach. These findings are likely to have implications for the procedural strategy in patients with NICM who are referred for VT ablation.

CLINICAL PERSPECTIVE

Ventricular tachycardia ablation in patients with nonischemic left ventricular cardiomyopathy is considered to be chal- lenging, which may partly because of the frequent intramural and subepicardial location of the arrhythmogenic substrate. Relatively little is known about typical scar patterns and its implications for the ablation strategy. In the present study, 19 consecutive patients with nonischemic cardiomyopathy who underwent contrast-enhanced MRI and ventricular tachycardia ablation are described. Two contrast-enhanced MRI–derived scar patterns (ie, basal anteroseptal and inferolateral) accounted for 89% of arrhythmogenic substrates, and 3 distinct 12-lead ECG morphologies of ventricular tachycardias were common and diagnostic for an underlying scar pattern. Basal anteroseptal scars were most effectively approached from the aortic root or basal anteroseptal left ventricular endocardium, and they were usually not well accessible from the epicardium, suggest- ing that an initial endocardial approach may be reasonable in these patients. In patients with inferolateral scars, however, an initial epicardial approach may be considered because epicardial ablation target sites were frequently identified in these patients. Endocardial electroanatomical voltage mapping could identify these scars only to a limited extent, with endocardial bipolar voltage only being affected when the scar involved the endocardial 2 mm and endocardial unipolar voltage when the scar involved the endocardial 4 mm and, less pronounced, by scar >4 mm from the endocardium. These findings provide insights into the arrhythmogenic substrate in patients with nonischemic cardiomyopathy and may have important practi- cal implications for preprocedural planning and intraprocedural substrate identification in patients undergoing ventricular tachycardia ablation.

REFERENCE LIST

1. Nakahara S, Tung R, Ramirez RJ, Michowitz Y, Vaseghi M, Buch E, Gima J, Wiener I, Mahajan A, Boyle NG, Shivkumar K. Characterization of the arrhythmogenic substrate in ischemic and nonischemic cardiomyopathy implications for catheter ablation of hemodynamically unstable ventricular tachycardia. J Am Coll Cardiol 2010;55(21):2355-65.
2. Haqqani HM, Tschabrunn CM, Tzou WS et al. Isolated septal substrate for ventricular tachycardia in nonischemic dilated cardiomyopathy: incidence, characterization, and implications. Heart Rhythm 2011;8(8): 1169-76.
3. Soejima K, Stevenson WG, Sapp JL, Selwyn AP, Couper G, Epstein LM. Endocardial and epicardial radiofrequency ablation of ventricular tachycardia associated with dilated cardiomyopathy: the importance of low-voltage scars. J Am Coll Cardiol 2004; 43(10):1834-42.
4. Tian J, Ahmad G, Mesubi O, Jeudy J, Dickfeld T. Three-dimensional delayed-enhanced cardiac MRI reconstructions to guide ventricular tachycardia ablations and assess ablation lesions. Circ Arrhythm Electrophysiol 2012;5(2):e31-e35.
5. Desjardins B, Morady F, Bogun F. Effect of epicardial fat on electroanatomical mapping and epicardial catheter ablation. J Am Coll Cardiol 2010;56(16):1320-7.
6. Hutchinson MD, Gerstenfeld EP, Desjardins B et al. Endocardial unipolar voltage mapping to detect epicardial ventricular tachycardia substrate in patients with nonischemic left ventricular cardiomyopathy. Circ Arrhythm Electrophysiol 2011;4(1):49-55.
7. van Huls van Taxis CF, Wijnmaalen AP, Piers SR, van der Geest RJ, Schalij MJ, Zeppenfeld K. Real-Time Integration of MDCT-Derived Coronary Anatomy and Epicardial Fat: Impact on Epicardial Electroanatomic Mapping and Ablation for Ventricular Arrhythmias. JACC Cardiovasc Imaging 2013;6(1):42-52.
8. Piers SR, van Huls van Taxis CF, Tao Q, van der Geest RJ, Askar SF, Siebelink HM, Schalij MJ, Zeppenfeld K. Epicardial substrate mapping for ventricular tachycardia ablation in patients with non-ischaemic cardiomyopathy: a new algorithm to differentiate between scar and viable myocardium developed by simultaneous integration of computed tomography and contrast-enhanced magnetic resonance imaging. Eur Heart J 2012;34(8):586-96.
9. Yokokawa M, Good E, Crawford T, Jongnarangsin K, Chugh A, Pelosi F, Jr., Oral H, Morady F, Bogun F. Ventricular tachycardia originating from the aortic sinus cusp in patients with idiopathic dilated cardiomyopathy. Heart Rhythm 2011;8(3):357-60.
10. Yamashina Y, Yagi T, Namekawa A, Ishida A, Sato H, Nakagawa T, Sakuramoto M, Sato E, Yambe T. Reentrant Ventricular Outflow Tract Tachycardia Arising from Focal Scar Detected by Delayed Enhancement Magnetic Resonance Imaging. Pacing Clin Electrophysiol 2012.
11. Mavrogeni S, Spargias C, Bratis C, Kolovou G, Markussis V, Papadopoulou E, Constadoulakis P, Papadimitropoulos M, Douskou M, Pavlides G, Cokkinos D. Myocarditis as a precipitating factor for heart failure: evaluation and 1-year follow-up using cardiovascular magnetic resonance and endomyocardial biopsy. Eur J Heart Fail 2011;13(8):830-7.
12. Corrado D, Basso C, Thiene G et al. Spectrum of clinicopathologic manifestations of arrhythmogenic right ventricular cardiomyopathy/dysplasia: a multicenter study. J Am Coll Cardiol 1997;30(6):1512-20.

13. Holmstrom M, Kivisto S, Helio T et al. Late gadolinium enhanced cardiovascular magnetic resonance of lamin A/C gene mutation related dilated cardiomyopathy. J Cardiovasc Magn Reson 2011;13(30.

14. Moon JC, Sachdev B, Elkington AG, McKenna WJ, Mehta A, Pennell DJ, Leed PJ, Elliott PM. Gadolinium enhanced cardiovascular magnetic resonance in Anderson-Fabry disease. Evidence for a disease specific abnormality of the myocardial interstitium. Eur Heart J 2003; 24(23):2151-5.